iScience

CellPress
OPEN ACCESS

Article

Late onset cardiovascular dysfunction in adult mice resulting from galactic cosmic ray exposure

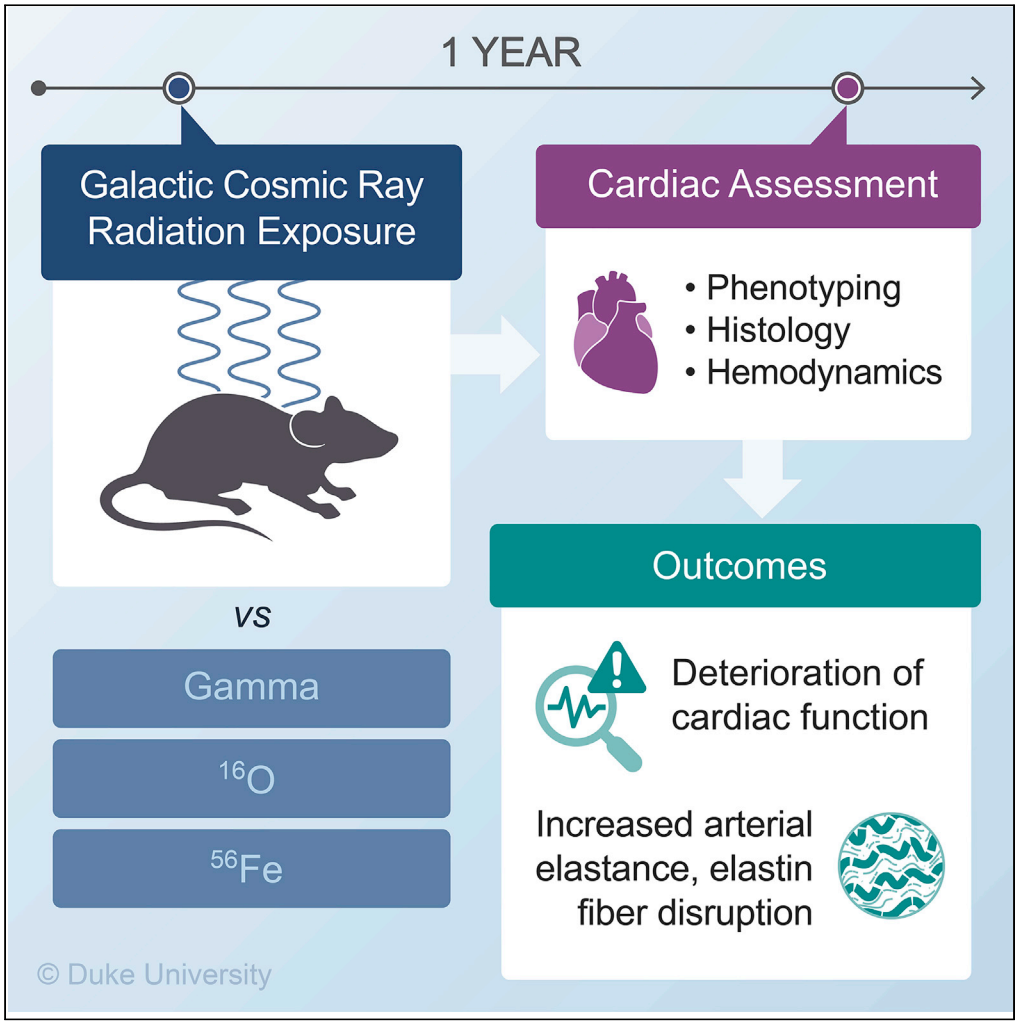

Muath Bishawi, Franklin H. Lee, Dennis M. Abraham, ..., Mark W. Dewhirst, George A. Truskey, Dawn E. Bowles

dawn.bowles@duke.edu

Highlights

Mice exposed to simplified galactic cosmic ray ($GCR_{5\text{-}ion}$) in controlled setting

Significant cardiovascular dysfunction 1year post exposure to $GCR_{5\text{-}ion}$

Increased arterial elastance, elastin fiber disruption in $GCR_{5\text{-}ion}$-exposed mice

Bishawi et al., iScience 25, 104086
April 15, 2022
https://doi.org/10.1016/j.isci.2022.104086

iScience

CellPress
OPEN ACCESS

Article

Late onset cardiovascular dysfunction in adult mice resulting from galactic cosmic ray exposure

Muath Bishawi,[1,2,8] Franklin H. Lee,[1,8] Dennis M. Abraham,[3] Carolyn Glass,[4] Stephanie J. Blocker,[5] Daniel J. Cox,[1] Zachary D. Brown,[1] Howard A. Rockman,[3] Lan Mao,[3] Tony C. Slaba,[6] Mark W. Dewhirst,[7] George A. Truskey,[2] and Dawn E. Bowles[1,9,*]

SUMMARY

The complex and inaccessible space radiation environment poses an unresolved risk to astronaut cardiovascular health during long-term space exploration missions. To model this risk, healthy male c57BL/6 mice aged six months (corresponding to an astronaut of 34 years) were exposed to simplified galactic cosmic ray ($GCR_{5\text{-}ion}$; 5-ion sim) irradiation at the NASA Space Radiation Laboratory (NSRL) at Brookhaven National Laboratories (BNL). Multi-modal cardiovascular functional assessments performed longitudinally and terminally revealed significant impairment in cardiac function in mice exposed to $GCR_{5\text{-}ion}$ compared to unirradiated controls, gamma irradiation, or single mono-energetic ions (^{56}Fe or ^{16}O). $GCR_{5\text{-}ion}$-treated mice exhibited increased arterial elastance likely mediated by disruption of elastin fibers. This study suggests that a single exposure to $GCR_{5\text{-}ion}$ is associated with deterioration in cardiac structure and function that becomes apparent long after exposure, likely associated with increased morbidity and mortality. These findings represent important health considerations when preparing for successful space exploration.

INTRODUCTION

Protected by the atmosphere as well as the magnetosphere, organisms living on the Earth do not encounter high levels of radiation from the space environment (Galactic Cosmic Rays [GCR] or Solar Particle Events [SPE]). Exploration to the Moon and Mars is expected to send humans beyond these protective barriers, for periods of months to years. While astronauts can be effectively shielded from most SPE exposures, highly energetic and complex GCR are difficult to shield and are considered a significant health risk for long-term exploration missions (Moeller et al., 2017). GCR consists primarily of high-energy protons and helium as well as a spectrum of high energy and charge (HZE) particles, such as ^{56}Fe and ^{16}O (Moeller et al., 2017). Exposures are predicted to occur at low fluence rates, with each cell in an astronaut's body being traversed by a proton every few days, by a helium nucleus every few weeks, and by a HZE nucleus once every few months, for a total dose of 0.3–0.6 mGy/day.(Nelson, 2016). Biological concerns associated with this environmental stress include cognitive and neurological dysfunction, carcinogenesis, immunological impairment, and cardiovascular degeneration (Cucinotta et al., 2011, 2017; Cucinotta, 2014; Parihar et al., 2015).

Modeling the impact of GCR exposure on the cardiovascular system has proven exceedingly difficult (Davis et al., 2021). Clinical and epidemiologic data obtained from studies of survivors of nuclear accidents, atomic bomb exposure, and radiation-based medical treatments have demonstrated that acute radiation exposure is associated with a higher rate of delayed cardiovascular-related morbidity and mortality (Ledsome, 2001; Taddeo and Armstrong, 2008; Baker et al., 2011; Adams et al., 2017; ; Abdelgawad et al., 2021). These studies are limited by confounding factors such as cancer comorbidity, follow-up time post radiation exposure, and estimations of radiation dose. Furthermore, none of these studies evaluate the effects of space radiation, and its unique characteristics, specifically.

Trying to understand the cardiovascular risk of space radiation exposure from astronaut data is also problematic because only 24 Apollo lunar astronauts have traveled beyond low earth orbit (LEO) into the complex space radiation environment. Of those individuals who have traveled beyond LEO, the amount of time

[1]Department of Surgery, Division of Surgical Sciences, Duke University Medical Center, MRSB1 Rm. 421b, 203 Research Drive, Durham, NC 27710, USA

[2]Department of Biomedical Engineering, Pratt School of Engineering, Durham, NC 27708, USA

[3]Department of Medicine, Duke University Medical Center, Durham, NC 27710, USA

[4]Department of Pathology, Duke University Medical Center, Durham, NC 27710, USA

[5]Department of Radiology, Duke University Medical Center, Durham, NC 27710, USA

[6]NASA Langley Research Center, Hampton, VA 23681, USA

[7]Radiation Oncology, Duke University Medical Center, Durham, NC 27710, USA

[8]These authors contributed equally

[9]Lead contact

*Correspondence: dawn.bowles@duke.edu

https://doi.org/10.1016/j.isci.2022.104086

spent there has been less than 50 days (Delp et al., 2016; Elgart et al., 2018). Despite being inside LEO, the recent NASA twin study demonstrated that, in comparison to the twin on Earth, the twin who inhabited the International Space Station for one year developed both genetic modifications (altered telomere length and DNA methylation) and markers of increased cardiovascular risk (carotid intima-media thickening and increase in the APOB/APOA1 ratio) (Garrett-Bakelman et al., 2019). However, the contribution of GCR to these complications is unclear, as such effects may be due to other stressors, such as microgravity.

Several investigations using the particle accelerator at BNL to deliver individual components of GCR (single mono-energetic ions such as protons, ^{56}Fe or ^{16}O) to healthy rodents have demonstrated only very minor changes in cardiac function at long-term endpoints. (Xinhua Yan et al., 2014b; Seawright et al., 2019). More sophisticated experimental design in which the sequence of fractionated doses of individual GCR components given over several days revealed dramatically different cardiovascular responses depending on the order of component delivery (Sasi et al., 2017; Seawright et al., 2019).

Recent technology development in engineering and physics at NSRL can now simulate the complex GCR environment over a short period of time to enable investigators to overcome the challenges associated with indirect assessment of possible GCR effects in the heart (Norbury et al., 2016; Simonsen et al., 2020). In our investigation, six-month- old C57BL/6 male mice were exposed to single mono-energetic ions or a simplified 5-ion GCR radiation protocol (referred to as $GCR_{5\text{-}ion}$ at NSRL), and longitudinal cardiac phenotyping was performed throughout the course of the study. Phenotyping strategies included transthoracic echocardiography (TTE), cardiac MRI (cMRI), and terminal pressure- volume loop assessment (PVL). It was hypothesized that exposure to simulated space radiation ($GCR_{5\text{-}ion}$) would result in increased deterioration of cardiac function compared to single mono-energetic ion exposures. This analysis demonstrates deterioration of cardiovascular function as reflected in histological and hemodynamic assessments one year after a single exposure to $GCR_{5\text{-}ion}$ whole body radiation. These perturbations may allude to the development of clinically diagnosable cardiovascular disease with further exposure to GCR or longer time post exposure.

RESULTS

Overall study design

The overall experimental design is provided in Figure 1. Prior to irradiation, c57BL/6 mice underwent baseline cardiac functional screening using transthoracic echocardiography (TTE). The mice were transported to BNL and, when at approximately 6 months of age, were exposed to the following radiation conditions: (a) 50, 100, or 200 cGy ^{137}Cs Gamma (0.662 MeV), (b) 15, 25, or 50 cGy ^{16}O (600 MeV/n), (c) 15, 25, or 50 cGy ^{56}Fe (1,000 MeV/n), or (d) 150 cGy $GCR_{5\text{-}ion}$ (H 1000 MeV/n, ^{28}Si 600 MeV/n, ^{4}He 250 MeV/n, ^{16}O 350 MeV/n, ^{56}Fe 600 MeV/n, and H 250 MeV/n) (Simonsen et al., 2020). Following radiation, exposed mice and age-matched unirradiated controls were returned to the home institution where cardiovascular measurements were acquired over time (Figures 1B–1D). Table S1 summarizes the study according to the number of animals evaluated by TTE, cMRI, or PVL and by radiation type and radiation dose.

The effect of different forms of radiation on cardiac function as assessed by transthoracic echocardiography (TEE)

To mimic conditions of assessment in astronauts, we performed conscious transthoracic echocardiography on all mice (Table S1). 24 echocardiography measurements were read or calculated for each animal, and measurements from animals in each radiation condition were compared to unirradiated controls (Table S2). Three experimental groups, $GCR_{5\text{-}ion}$ (Figure 2 and Table S3), ^{56}Fe (Figure S1 and Table S4), and ^{16}O (Figure S2 and Table S5), demonstrated statistically significant changes in the echocardiographic measure of cardiac function as assessed by fractional shortening (FS) and calculated ejection fraction (EF). Both these measures of systolic function were elevated in a small but statistically significant manner in $GCR_{5\text{-}ion}$-exposed animals (Figures 2A and 2B). Additionally, a small but statistically significant elevation in heart rate was observed in $GCR_{5\text{-}ion}$-exposed animals compared to unirradiated controls after one year (Figure 2C). Measures of early and late diastolic function (E/A, IVRT, E′) were not statistically different between GCR-treated animals and controls (Figures 2D–2F), nor were they different in animals exposed to ^{56}Fe, ^{16}O, or Gamma (Figures S1–S3, respectively). Differences in systolic function and heart rate (HR) in $GCR_{5\text{-}ion}$-exposed animals, while significant, were modest and of unclear physiological relevance. For instance, the median difference in percent FS between $GCR_{5\text{-}ion}$ and unirradiated controls was −2.8 (95% CI -5.4 to −0.36). The same was true for EF, with a median difference of −3.4 (95% CI -6.1 to −0.30). There were also minimal differences in HR and systolic functional assessments between age control

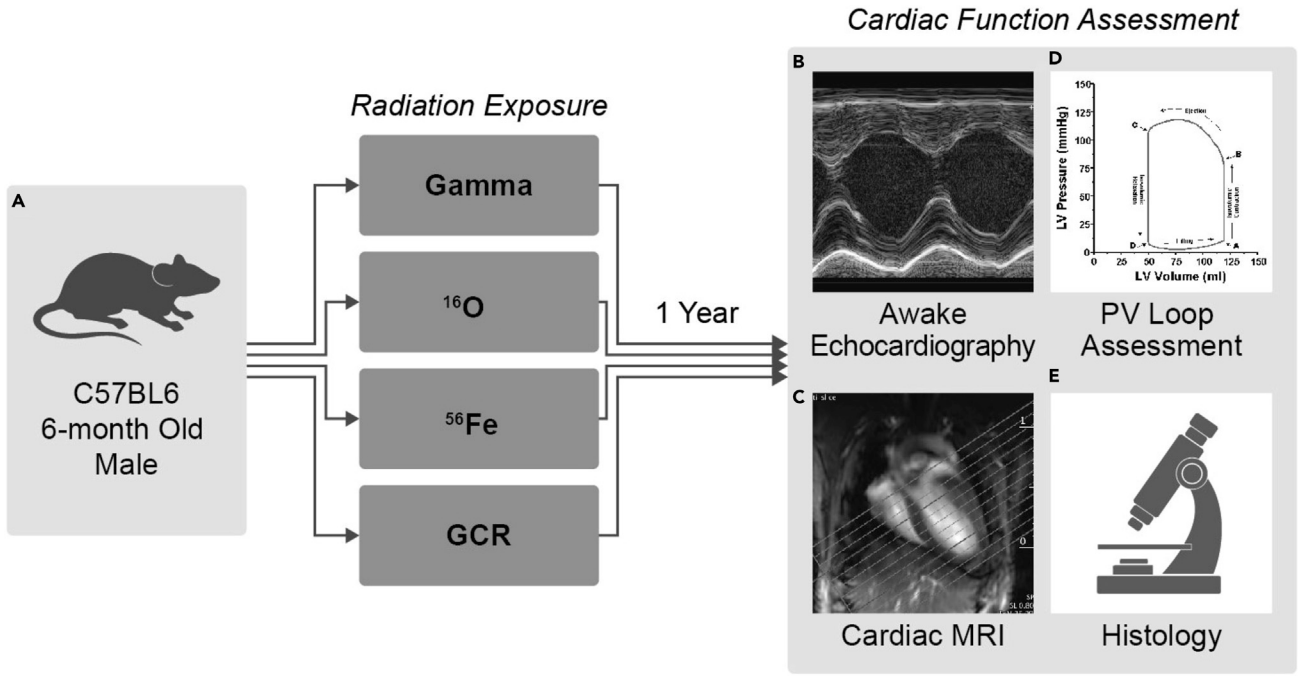

Figure 1. Overall experimental design

(A) Experimental set up included c57BL/6 mice undergoing radiation at six months of age with sham radiation controls These included ^{137}Cs Gamma radiation with an escalating dose 50–200cGy, ^{16}O (15–50cGy) 600 MeV/n, ^{56}Fe (15–50cGy) 1,000 MeV/n, and galactic cosmic rays ($GCR_{5\text{-ion}}$) (150 cGy that included H 1000 MeV/n, ^{28}Si 600 MeV/n, ^{4}He 250 MeV/n, ^{16}O 350 MeV/n, ^{56}Fe 600 MeV/n, H 250 MeV/n). Detailed list of mouse per exposure type, dose, and assessment modality available in Table S1. One year post radiation assessments of cardiac function included the following: (B) awake echocardiography acquisition of M-mode images, B-mode, and Doppler images not depicted; (C) sedated cardiac MRI without contrast; (D) terminal pressure-volume loop assessment and analysis; (E) and cardiac/aortic histology analysis of H&E and MT stained sections.

animals, and those exposed to ^{56}Fe (Figures S1A–S1C), ^{16}O (Figures S2A–S2C), or Gamma (Figures S3A–S3C), at one year post radiation. This was also true for measures of diastolic function from mice exposed to ^{56}Fe, ^{16}O, or Gamma radiation, respectively (Figures S1–S3D, S3E, and S3F).

To further characterize *in vivo* changes in cardiac structure and function associated with $GCR_{5\text{-ion}}$ radiation, a subset of animals underwent preclinical cMRI evaluation (Figure S4). cMRI imaging including temporal "heart movie" acquisitions, providing images of the heart at 12 time points per cardiac cycle. While there appears to be no difference in stroke volume (SV) and LV thickness during systole, a small difference was detected in end-diastole LV thickness of $GCR_{5\text{-ion}}$ animals compared to controls (difference of 0.13mm, 95% CI -0.24 to −0.01, p = 0.032) (Figure S4C). However, when the same measurements were made during systole, no difference was seen between the groups. Further, when comparing the dynamic change in LV wall thickness from systole to end-diastole, no trends appeared between $GCR_{5\text{-ion}}$ -exposed and control animals. Finally, changes in cardiac volumes across the cardiac cycle between the groups appeared to be similar (Figure S4E).

Cardiac pressure-volume loop (PVL) analyses reveal decreased systolic function and increased arterial elastance one year after $GCR_{5\text{-ion}}$ but not after ^{56}Fe, ^{16}O, or Gamma radiation exposure

Hemodynamic assessment via pressure-volume loop (PVL) analysis is considered the gold standard for evaluating load-dependent and -independent measures of cardiac contractile function (Abraham and Mao, 2015). At one year post radiation, a subset of animals from each study group ($GCR_{5\text{-ion}}$, ^{56}Fe, ^{16}O, Gamma, and control) underwent cardiac evaluation using cardiac PVL analyses (Table S7 lists all PVL parameters measured or calculated; Tables S8 and S9 lists average PVL parameter values for 150 cGy $GCR_{5\text{-ion}}$ and single mono-energetic ion cohorts, respectively).

Mice that had been exposed to 150 cGy of $GCR_{5\text{-ion}}$ demonstrated significant diminishment in load-dependent measures of cardiac function, including stroke work (SW) (Figure 3A), stroke volume (SV) (Figure 3B),

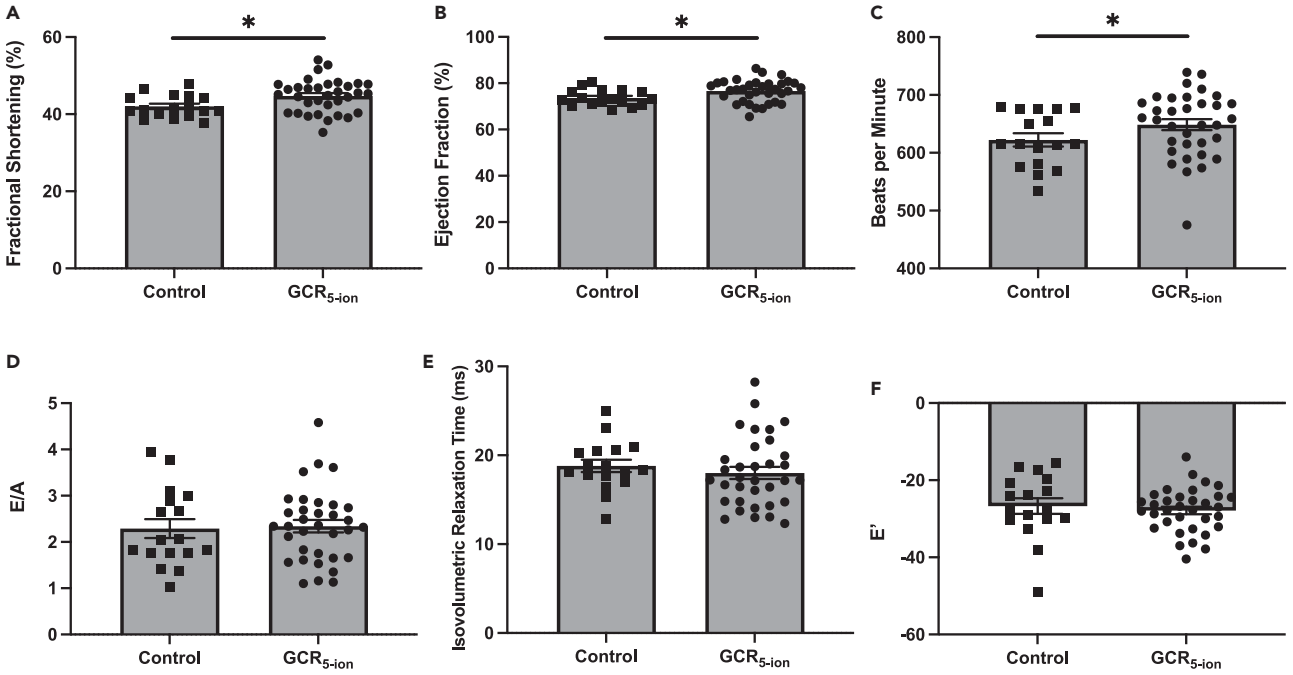

Figure 2. Echocardiographic measurements of unirradiated age-matched control and 150 cGy $GCR_{5\text{-ion}}$-treated animals one year post radiation

Fractional shortening (A), ejection fraction (D), heart rate (C), early to late filling of mitral inflow (D), isovolumetric relaxation time (E), and passive LV filling (F). N = 17 for controls, and N = 34 for $GCR_{5\text{-ion}}$ animals. Nonparametric Mann-Whitney test, 2 sided. *$p \leq 0.05$, **$p \leq 0.01$. Data are represented as mean $\pm$ SEM.

and cardiac output (CO) (Figure 3C). Of note, some load-dependent measure of systolic function (dP/dt max and Ejection Fraction) was not significantly different between $GCR_{5\text{-ion}}$ and unirradiated control (Figures 3D and 3E). However, the load-independent measurement, preload recruitable stroke work (PRSW), was significantly reduced in $GCR_{5\text{-ion}}$-exposed animals (Figure 3F). In this instance, the median difference of PRSW between $GCR_{5\text{-ion}}$ and unirradiated control was −25.21% (95%CI, −48.41% to −11.74%). Early diastolic filling time, quantified by Tau, was not different between the groups (Figure 3G). Peripheral vascular resistance, measured by arterial elastance (Ea), was significantly increased in $GCR_{5\text{-ion}}$-treated animals as compared to controls (Figure 3H). Echocardiography characteristics of PVL-evaluated mice were compared to that of the larger cohort, showing similar echocardiography characteristics between the two groups (Figure S5).

Despite the robust impact on cardiac function as measured by PVL, $GCR_{5\text{-ion}}$ exposure did not significantly alter mortality (Figure S6) or other general indicators of overall health such as blood pressure (Figures S7A–S7C) or weight (Figure S7D) compared to controls at 1 year post radiation.

In contrast to the $GCR_{5\text{-ion}}$-irradiated animals, no meaningful differences in systolic or diastolic performance from PVL analysis (SW, SV, CO, EF, dP/dTmax, PRSW, Tau, or Ea) were noted during the one-year analysis post 50 cGy ^{56}Fe, 50 cGy ^{16}O, or 200 cGy Gamma radiation compared to age-matched controls (Figure S8).

GCR radiation associated with changes in aortic elastic fiber organization

The PVL evaluation of $GCR_{5\text{-ion}}$ mice suggested enhanced peripheral vascular resistance and no significant differences in cardiac morphology. To correlate these functional studies caused by $GCR_{5\text{-ion}}$ exposure with anatomic and cellular changes, heart and aortic tissues from a subset of animals receiving $GCR_{5\text{-ion}}$ and controls underwent histological evaluation. While there was no significant change in cardiac fibrosis between groups (data not shown), evaluation of the thoracic aorta revealed an overall increase in medial necrosis, medial degeneration, elastin fragmentation, and architectural distortion (Figure 4). In particular, $GCR_{5\text{-ion}}$ mice exhibited a higher average grading of medial necrosis, elastin fragmentation, and

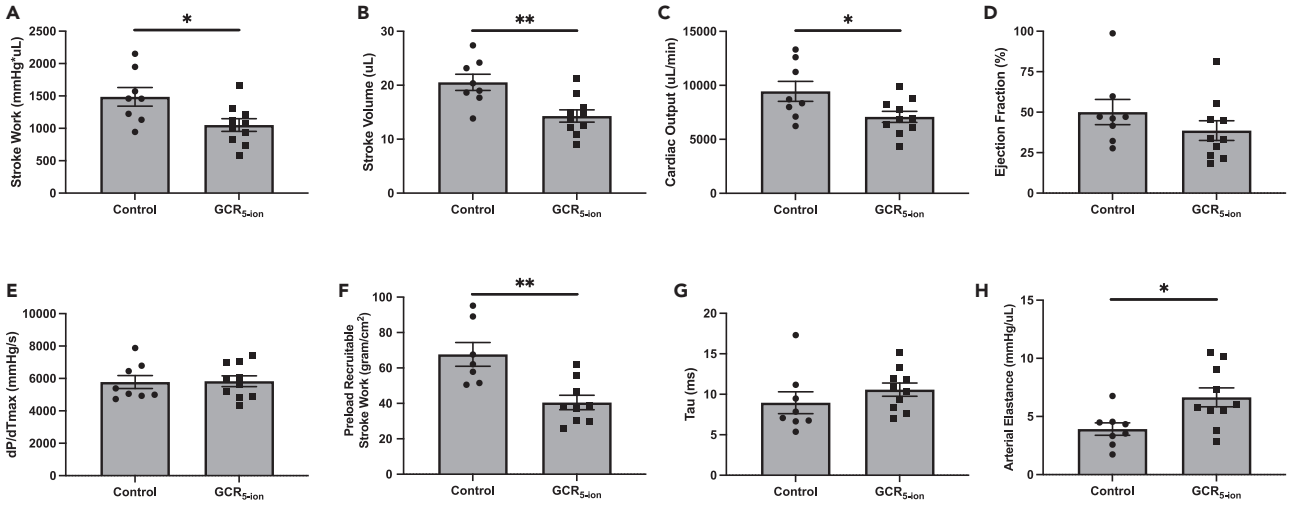

Figure 3. Pressure-volume loop (PVL) hemodynamic measurements of age-matched unirradiated control and $GCR_{5\text{-}ion}$-treated c57BL/6 mice one year post radiation

Stroke work (A), stroke volume (B), cardiac output (C), ejection fraction (D), changes in LV pressure over time (E), preload recruitable stroke work (F), left ventricular relaxation time constant (G), and arterial elastance (H). N = 8 for controls, and 9–10 for GCR animals. Nonparametric Mann-Whitney test, 2 sided. *$p \leq 0.05$, **$p \leq 0.01$. Data are represented as mean ± SEM.

architectural distortion (Figures 4A, 4C, and 4D), but showed lower average grading for medial degeneration (Figure 4B). Masson trichrome (MT)-stained mouse aortas exposed to $GCR_{5\text{-}ion}$ showed signs of elastin fragmentation (Figure 4E and 4F) while unirradiated age-matched control did not have any observable instances (Figure 4G).

Western Blot (WB) analysis of heart apex tissue reveal changes in cardiac markers 1 year post-$GCR_{5\text{-}ion}$ radiation exposure

Heart apex tissue of 150 cGy $GCR_{5\text{-}ion}$-irradiated mice and unirradiated age-matched controls were screened for the following cardiac markers: Fibulin-4, Fibulin-5, TGF-β1, and eGFR (Figures S10 and S11). Fibulin-4, Fibulin-5, and eGFR expression in $GCR_{5\text{-}ion}$-irradiated mice were decreased compared to age-matched unirradiated control; eGFR was the only marker that showed a statistically significant decrease compared to controls. On the contrary, TGF-β1 expression was increased in $GCR_{5\text{-}ion}$-irradiated mice when compared to age-matched unirradiated controls, which was not statistically significant.

DISCUSSION

We report changes in resting load-dependent and -independent measures of cardiac function, as well as resting arterial elastance, one year after exposure of mice to $GCR_{5\text{-}ion}$ radiation. Further, changes in arterial elastance appear to be related to long-term damage in aortic elastin fibers. Reduced cardiac contractility and increased peripheral vascular resistance, key hemodynamic altertions in human congestive heart failure, can result from one exposure of $GCR_{5\text{-}ion}$ radiation.

There have been several animal studies that simulated the effect of terrestrial and space radiation scenarios on cardiac function (Monceau et al., 2013; X. Yan et al., 2014a; Hughson et al., 2018; Seawright et al., 2019). However, available studies to date have been limited by short follow-up times and methods for evaluating cardiac function preclinically. In addition, no study has evaluated the effects of the complex radiation scenarios that are likely to be experienced during extended periods in space, such as GCR. To study this unique radiation environment, particle accelerators have been used to generate single mono-energetic ion beams at fixed energies; however, space radiation is much more complex, with a mixture of ion species and energies. Recently, GCR simulation became possible at NSRL, enabling the current report (Simonsen et al., 2020).

In this study, we utilized multiple modalities to assess cardiac function in mice (TTE, PVL, and cMRI), one year after exposure to $GCR_{5\text{-}ion}$. We chose a comprehensive approach for cardiac evaluation,

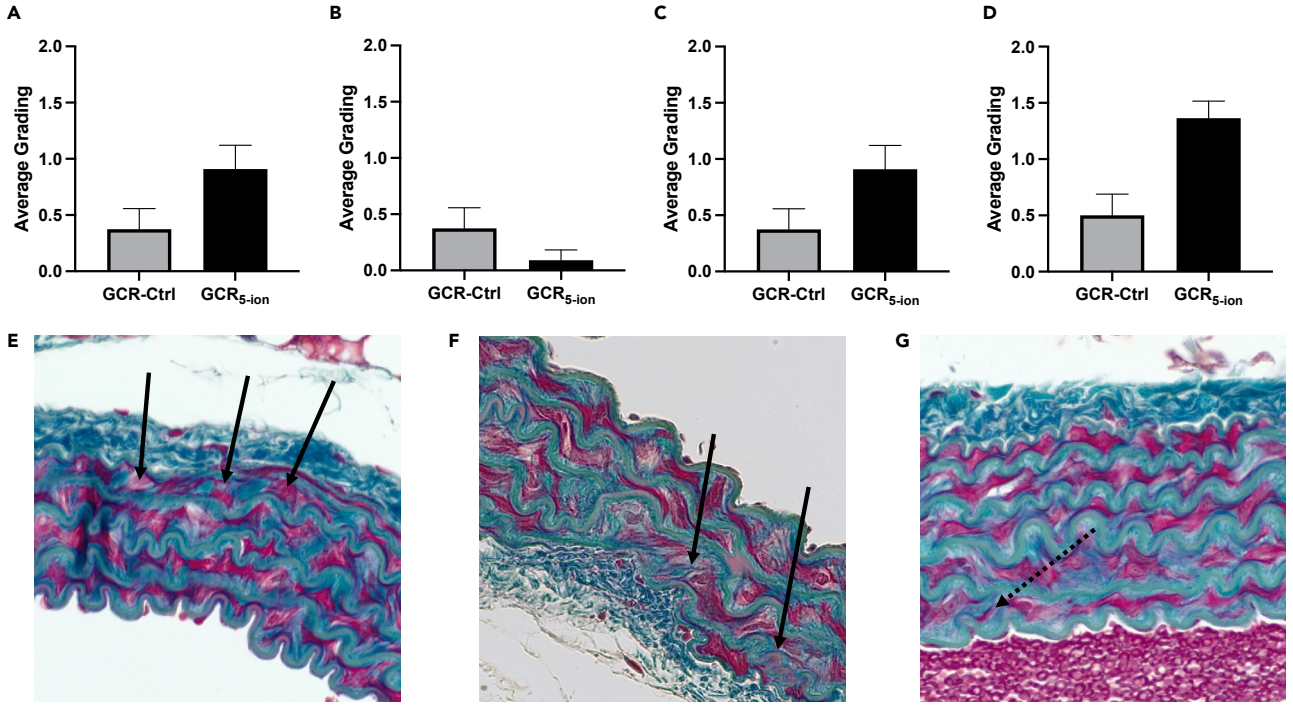

Figure 4. Average histological grading and aortic Masson trichrome staining of 150 cGy $GCR_{5\text{-}ion}$ compared to GCR controls one year post radiation

Medial necrosis (A), medial degeneration (B), elastin fragmentation (C), and architectural distortion (D), 150cGy $GCR_{5\text{-}ion}$ mouse aortas (E, F), and GCR control (G). Solid black arrows point to areas of focal elastin fragmentation (E, F). Bridging between elastin fibers depicted by dotted black arrows (G). N = 11 for 150cGy $GCR_{5\text{-}ion}$ and N = 8 GCR controls. Data are represented as mean ± SEM.

understanding the limitations of each test and the need to compare measures across modalities for validation. While transthoracic echocardiography is frequently employed in mouse studies, it may lack the sensitivity required to reveal the impact of space radiation on cardiovascular function (Sato et al., 2001; Hughson et al., 2018). A review of the literature revealed two common pitfalls. First, most studies used healthy wild-type mice and sedated echocardiography as the primary method of cardiac assessment. These experiments may be affected by the cardiodepressant properties of sedation. Second, many prior studies used only one echocardiography reader or unclear prior internal validation of reads. This becomes a problem when faced with the large variability encountered in mouse echocardiograms (Gao et al., 2011).

We performed echocardiograms on conscious mice, which were then analyzed independently by two clinicians blinded to exposure conditions. Despite identifying large and clinically meaningful differences in cardiac function after $GCR_{5\text{-}ion}$ using PVL testing, echocardiography was unable to discriminate between groups. This may explain inconsistencies in the current preclinical literature when echocardiography is used as the primary method of cardiac functional assessment. Given the known effect of anesthesia on cardiac function, we did not employ anesthesia for echocardiography (Gao et al., 2011). This is an important divergence from the majority of reports today, in which echocardiography is performed under sedation (Hughson et al., 2018). Isoflurane induces a negative inotropic effect on cardiac function (Gao et al., 2011), which may mask subtle differences related to the treatment. Although $GCR_{5\text{-}ion}$ -exposed animals exhibited statistically significant elevation of FS and EF (Figures 2A and 2B), we determined that the force-frequency effect, a known contributor to cardiac function, was not the likely cause after plotting FS against FS/HR (Figure S9). As $GCR_{5\text{-}ion}$ -exposed animals' values did not diverge from that of their respective controls, we suggest that the elevation observed in FS and EF was due to differing loading conditions between groups, possibly related to higher fluid intake.

Pressure-volume testing demonstrated consistent changes in measures of load-dependent and -independent systolic function for $GCR_{5\text{-}ion}$ -exposed animals after one year. The reduction in hemodynamically related load-dependent measures of stroke volume, stroke work, and cardiac output could be explained

by an increase in afterload (elevated arterial elastance) and a reduction in contractility (decreased preload recruitable stroke work). In light of these findings, the apparent lack of effect of $GCR_{5\text{-}ion}$ on peripherally measured tail cuff blood pressures could be explained by the combined effects of increased peripheral vascular resistance (raises blood pressure) and reduced cardiac contractility (reduces blood pressure). The observed changes in arterial elastance in $GCR_{5\text{-}ion}$-exposed animals correspond to clinical studies that demonstrate arterial stiffness after radiation exposure in humans (Gujral et al., 2016). Furthermore, the alterations in arterial elastance could be explained by disruption of arterial elastic fiber integrity (Yanagisawa and Wagenseil, 2019) and organization for the $GCR_{5\text{-}ion}$-exposed animals as compared to age-matched control animals. While aging is associated with measurable changes in the integrity of aortic elastic fibers (Fhayli et al., 2020), $GCR_{5\text{-}ion}$ animals demonstrated significant deterioration 1 year post exposure, even when age was considered with matched controls. Elastic fiber integrity is critical for the Windkessel effect, a necessary process for blood pressure regulation and secondary organ blood flow (Belz, 1995). Taken together, these data suggest that astronauts exposed to GCR may suffer damage to both vascular and cardiac tissues that may predispose them to conditions such as congestive heart failure.

Western blot analysis of cardiac markers in heart apexes from $GCR_{5\text{-}ion}$-irradiated mice showed changes in protein expression, suggestive of changes in the extracellular matrix of the heart tissue. In particular, decreased eGFR expression, which is implicated in TGF-β1-mediated fibrosis, may explain the lack of fibrosis seen on histological assessment of $GCR_{5\text{-}ion}$-irradiated mice heart tissue. To provide further insight into the molecular changes post $GCR_{5\text{-}ion}$ irradiation, a proteomics analysis of heart tissue and plasma is currently in progress.

In this study, we report maladaptive changes in cardiac structure and function one year after exposure to $GCR_{5\text{-}ion}$ compared to age-matched controls. These effects were only seen in $GCR_{5\text{-}ion}$ -exposed animals, and were not found in animals exposed to single mono-energetic ion or gamma radiation. NASA estimates that a trip to Mars and back to Earth would expose the astronauts to a total accumulated dose of 50–75 cGy of GCR irradiation. We acknowledge using a GCR dose of 150 cGy, which is about 2 times the maximum dose that is estimated, an astronaut will be exposed to in future deep space missions. While these doses used in the study were higher than the dose expected during mission, the doses were reviewed and approved by NASA. The intention of the current study was not to quantify risks in an animal model and directly use this information for decision making for space exploration. Rather, the information reported here will be integrated with other experiments as well as with human epidemiology data in order to develop a full understanding as well as quantitative risk models.

These findings have important implications for current and future plans of deep space exploration by NASA. Because we found a deterioration in cardiac structure and function after a single exposure to GCR, a reasonable approach to prolonged human space flight would be for astronauts to have an assessment of cardiac function by echocardiography and/or cMRI, prior to, immediately after, and several months following space flight. High-resolution noninvasive cardiac imaging before and after space travel would likely be best carried out as a clinical trial testing whether brief or prolonged space travel affects short or long-term cardiac function and cardiopulmonary functional capacity.

Limitations of the study

This was also the first report to use cMRI to evaluate cardiac structure and function post exposure to space radiation. cMRI provides unique opportunities for assessing a number of cardiac functional and structural characteristics (Gardner et al., 2009). Two important limitations with our early cMRI studies were the small group size and the lack of contrast agent. The latter, while not prohibitive, can reduce the accuracy of measurements due to lower contrast at the blood-to-wall boundary, particularly during diastole. Because of these considerations, preclinical cMRI may still represent a sensitive means of understanding murine cardiac structure and function post space radiation in healthy animals and this methodology may prove useful in future should we identify a group which shows the largest differences in echo.

STAR★METHODS

Detailed methods are provided in the online version of this paper and include the following:

- KEY RESOURCES TABLE
- RESOURCE AVAILABILITY

SUPPLEMENTAL INFORMATION

Supplemental information can be found online at https://doi.org/10.1016/j.isci.2022.104086.

ACKNOWLEDGMENTS

We would like to thank members of NSRL Peter Guida, PhD, Adam Rusek, PhD, James Jardine, Paula Bennet, Michael Sievert, and Deborah Snyder. We would also like to acknowledge Duke DLAR and all the individuals that help to care for our animals over the long study period. Additionally, we would like to thank the Duke Cardiovascular Physiology Core and the Mandel Center for Hypertension and Atherosclerosis for their support in all mouse cardiovascular phenotyping. We would like to thank G. Allan Johnson, Director of the Duke Center for In Vivo Microscopy for has expertise and guidance in our assessment of cMRI. This work is supported by NASA research grant NNX16AK20G to DEB, Translational Research Institute though NASA copperative agreement NNX16AK20G to DEB, National Institutes of Health 100000002grants NIH-NHLBI 1R38HL143612-01 to M.B., 1K08HL125905-01 to D.M. A, and HL056687 and HL075443 to H.A.R. This manuscript is dedicated by the authors to six-year-old Nicholas (Nicky) Abraham and his mother Julie Abraham, lovers of all things NASA and space. While they left this earth way too soon, we know their light is travelling among the stars.

AUTHOR CONTRIBUTIONS

Conceptualization, Methodology (DEB, MB, GAT, DMA, HAR, MWD, TCS); Formal Analysis (MB, FHL, DMA, CG); Investigation (MB, FHL, DMA, CG, LM, SJB, DEB, DJC, ZDB); Data Curation (FHL); Writing—Original Draft (MB, FHL, DEB, GAT, DMA, HAR, TCS, CG, SJB, ZDB, MWD); Writing—Review & Editing (MB, FHL, DEB, GAT, DMA, HAR, TCS, CG, SJB, ZDB, MWD, HAR); Visualization (MB, FHL), Supervision (DEB, HAR); Project Administration, Funding Acquisition (DEB)

DECLARATION OF INTERESTS

The authors declare no competing interests.

Received: September 25, 2021
Revised: January 16, 2022
Accepted: March 11, 2022
Published: April 15, 2022

REFERENCES

Abdelgawad, I.Y., Sadak, K.T., Lone, D.W., Dabour, M.S., Niedernhofer, L.J., and Zordoky, B.N. (2021). Molecular mechanisms and cardiovascular implications of cancer therapy-induced senescence. Pharmacol. Ther. *221*, 107751. https://doi.org/10.1016/j.pharmthera.2020.107751.

Abraham, D., and Mao, L. (2015). Cardiac pressure-volume loop analysis using conductance catheters in mice. J. Vis. Exp. 52942. https://doi.org/10.3791/52942.

Abraham, D.M., Davis, R.D., Warren, C.M., Mao, L., Wolska, B.M., Solaro, R.J., and Rockman, H.A. (2016). β-Arrestin mediates the Frank–Starling mechanism of cardiac contractility. Proc. Natl. Acad. Sci. *113*, 14426–14431. https://doi.org/10.1073/PNAS.1609308113.

Abraham, D.M., Lee, T.E., Watson, L.J., Mao, L., Chandok, G., Wang, H.G., Frangakis, S., Pitt, G.S., Shah, S.H., Wolf, M.J., and Rockman, H.A. (2018). The two-pore domain potassium channel TREK-1 mediates cardiac fibrosis and diastolic dysfunction. J. Clin. Invest. *128*, 4843–4855. https://doi.org/10.1172/JCI95945.

Adams, H., et al. (2017). Radiation therapy induced cardiovascular disease. Heart Vessels Transplant. https://doi.org/10.24969/hvt.2017.25.

Baker, J.E., Moulder, J.E., and Hopewell, J.W. (2011). Radiation as a risk factor for cardiovascular disease. Antioxid. Redox Signaling *1*, 1945–1956. https://doi.org/10.1089/ars.2010.3742.

Belz, G.G. (1995). Elastic properties and Windkessel function of the human aorta. Cardiovasc. Drugs Ther *9*, 73–83. https://doi.org/10.1007/BF00877747.

Brown, Z.D., Bishawi, M., Roan, J., Lee, F., Nevo, A., Watson, M., and Bowles, D.E. (2020). The use of an inexpensive processing aid device (the Mouse PAD) to facilitate rodent tissue banking. Bio. Techniques *69*, 364–368. https://doi.org/10.2144/BTN-2019-0069.

Cucinotta, F.A. (2014). Space radiation risks for astronauts on multiple international space station missions. PLoS One *9*, 96099. https://doi.org/10.1371/journal.

Cucinotta, F.A., Kim, M.-H.Y., and Chappell, L.J. (2011). Space radiation cancer risk projections and uncertainties-2010. http://www.sti.nasa.gov.

Cucinotta, F.A., To, K., and Cacao, E. (2017). Predictions of space radiation fatality risk for exploration missions. Life Sci. Space Res. *13*, 1–11. https://doi.org/10.1016/j.lssr.2017.01.005.

Davis, C.M., Allen, A.R., and Bowles, D.E. (2021). Consequences of space radiation on the brain and cardiovascular system. J. Environ. Sci. Health C: Toxicol. Carcinogenesis *39*, 180–218. https://doi.org/10.1080/26896583.2021.1891825.

Delp, M.D., Charvat, J.M., Limoli, C.L., Globus, R.K., and Ghosh, P. (2016). Apollo lunar astronauts show higher cardiovascular disease mortality: possible deep space radiation effects on the vascular endothelium. Sci. Rep. *6*, 29901. https://doi.org/10.1038/srep29901.

Elgart, S.R., Little, M.P., Chappell, L.J., Milder, C.M., Shavers, M.R., Huff, J.L., and Patel, Z.S. (2018). Radiation exposure and mortality from cardiovascular disease and cancer in early NASA astronauts. Sci. Rep. *8*, 8480. https://doi.org/10.1038/s41598-018-25467-9.

Fhayli, W., Boëté, Q., Kihal, N., Cenizo, V., Sommer, P., Boyle, W.A., Jacob, M., and Faury, J. (2020). Dill extract induces elastic fiber neosynthesis and functional improvement in the ascending aorta of aged mice with reversal of age-dependent cardiac hypertrophy and involvement of lysyl oxidase-like-1. Biomolecules *10*, 173. https://doi.org/10.3390/biom10020173.

Gao, S., Ho, D., Vatner, D.E., and Vatner, S.F. (2011). Echocardiography in mice. Curr. Protoc. mouse Biol. *1*, 71–83. https://doi.org/10.1002/9780470942390.mo100130.

Gardner, B.I., Bingham, S.E., Allen, M.R., Blatter, D.D., and Anderson, J.L. (2009). Cardiac magnetic resonance versus transthoracic echocardiography for the assessment of cardiac volumes and regional function after myocardial infarction: an intrasubject comparison using simultaneous intrasubject recordings. Cardiovasc. Ultrasound *7*, 38. https://doi.org/10.1186/1476-7120-7-38.

Garrett-Bakelman, F.E., Darshi, M., Green, S.J., Gur, R.C., Lin, L., Macias, B.R., McKenna, M.J., Meydan, C., Mishra, T., et al. (2019). The NASA twins study: a multidimensional analysis of a year-long human spaceflight. Science *364*, eaau8650. https://doi.org/10.1126/science.aau8650.

Gujral, D.M., Shah, B.N., Chahal, N.S., Bhattacharyya, S., Senior, R., Harrington, K.J., Nutting, C.M., et al. (2016). Arterial stiffness as a biomarker of radiation-induced carotid atherosclerosis. Angiology *67*, 266–271. https://doi.org/10.1177/0003319715589520.

Hughson, R.L., Helm, A., and Durante, M. (2018). Heart in space: effect of the extraterrestrial environment on the cardiovascular system. Nat. Rev. Cardiol. *15*, 167–180. https://doi.org/10.1038/nrcardio.2017.157.

Ledsome, J.R. (2001). Summary of final report: space Life Sciences planning workshop (SLSPW). June 5-7, 2000 mont Tremblant, Quebec. Can. J. Physiol. Pharmacol. *79*, 741–743. https://doi.org/10.1139/cjpp-79-9-741.

Moeller, R., Raguse, M., Leuko, S., Berger, T., Hellweg, C.E., Fujimori, A., Okayasu, R., and Horneck, G.; the STARLIFE Research Group (2017). STARLIFE -An international campaign to study the role of galactic cosmic radiation in astrobiological model systems. Astrobiology *17*, 101–109. https://doi.org/10.1089/ast.2016.1571.

Monceau, V., Meziani, L., Strup-Perrot, C., Morel, E., Schmidt, M., Haagen, J., Escoubet, B., Dörr, W., and Vozenin, M. (2013). Enhanced sensitivity to low dose irradiation of ApoE-/- mice mediated by early pro-inflammatory profile and delayed activation of the TGFβ1 cascade involved in fibrogenesis. PLoS One *8*, e57052. https://doi.org/10.1371/journal.pone.0057052.

Nelson, G.A. (2016). Space radiation and human exposures, A primer. Radiat. Res. *185*, 349–358. https://doi.org/10.1667/RR14311.1.

Norbury, J.W., Schimmerling, W., Slaba, T.C., Azzam, E.I., Badavi, F.F., Baiocco, G., Benton, E., Bindi, V., Blakely, E.A., Blattnig, S.R., et al. (2016). Galactic cosmic ray simulation at the NASA space radiation laboratory. Life Sci. Space Res. *8*, 38–51. https://doi.org/10.1016/j.lssr.2016.02.001.

Parihar, V.K., Allen, B., Tran, K.K., Macaraeg, T.G., Chu, E.M., Kwok, S.F., Chmielewski, N.N., Craver, B.M., Baulch, J.E., Acharya, M.M., et al. (2015). What happens to your brain on the way to Mars. Sci. Adv. *1*, e1400256. https://doi.org/10.1126/sciadv.1400256.

Sasi, S.P., Yan, X., Zuriaga-Herrero, M., Gee, H., Lee, J., Mehrzad, R., Song, J., Onufrak, J., Morgan, J., Enderling, H., et al. (2017). Different sequences of fractionated low-dose proton and single iron-radiation-induced divergent biological responses in the heart. Radiat. Res. *188*, 191–203. https://doi.org/10.1667/RR14667.1.

Sato, Y., Schmidt, A.G., Kiriazis, H., Hoit, B.D., Kranias, E.G., et al. (2001). Letter to the editor: Re-evaluation of heart failure in transgenic mice with impaired SR Ca2+ release. J. Mol. Cell Cardiol. *33*, 1757–1759. https://doi.org/10.1006/jmcc.2001.1430.

Seawright, J.W., et al. (2019). Effects of low-dose oxygen ions and protons on cardiac function and structure in male C57BL/6J mice. Life Sci. Space Res. *20*, 72–84. https://doi.org/10.1016/j.lssr.2019.01.003.

Simonsen, L.C., Slaba, T.C., Guida, P., and Rusek, A. (2020). NASA' s first ground-based Galactic Cosmic Ray Simulator : enabling a new era in space radiobiology research. PLoS Biol. *18*, e3000669. https://doi.org/10.1371/journal.pbio.3000669.

Taddeo, T.A., and Armstrong, C.W. (2008). Spaceflight medical systems. In Principles of Clinical Medicine for Space Flight (Springer), pp. 201–231.

Yan, X., Sasi, S.P., Gee, H., Lee, J., Yang, Y., Song, J., Carrozza, J., and Goukassian, D.A. (2014a). Radiation-associated cardiovascular risks for future deep-space missions. J. Radiat. Res. *55* (suppl 1), i37–i39. https://doi.org/10.1093/jrr/rrt202.

Yan, Xinhua, Sasi, S.P., Gee, H., Lee, J., Yang, Y., Mehrzad, R., Onufrak, J., Song, J., Enderling, H., Agarwal, A., et al. (2014b). Cardiovascular risks associated with low dose ionizing particle radiation. PLoS One *9*, e110269. https://doi.org/10.1371/journal.pone.0110269.

Yanagisawa, H., and Wagenseil, J. (2019). Elastic fibers and biomechanics of the aorta: insights from mouse studies. Matrix Biol. https://doi.org/10.1016/j.matbio.2019.03.001.

Yoo, B.S., Lemaire, A., Mangmool, S., Wolf, M.J., Curcio, A., Mao, L., and Rockman, H.A. (2009). β1-Adrenergic receptors stimulate cardiac contractility and CaMKII activation in vivo and enhance cardiac dysfunction following myocardial infarction. Am. J. Physiol. - Heart Circulatory Physiol. *297*, H1377–H1386. https://doi.org/10.1152/ajpheart.00504.2009.

STAR★METHODS

KEY RESOURCES TABLE

REAGENT or RESOURCE	SOURCE	IDENTIFIER
Antibodies		
Rabbit Anti-Fibulin 5 pAb	Thermo Fisher	CAT#12188-1-AP; RRID: AB_2105939
Rabbit Anti-TGF-β1 mAb	Abcam	Product code ab215715; RRID: AB_2893156
Rabbit Anti-eGFR mAb	Abcam	Product code ab52894; RRID: AB_869579
Goat Anti-Rabbit IgG (H + L)-HRP Conjugate	Bio-Rad	CAT# 1706515; RRID: AB_11125142
Rabbit Anti-Fibulin 4 pAb	Thermo Fisher	CAT# BS-13059R
Biological samples		
Mouse: C57BL/6J male heart tissue	Bowles Lab (Duke University); this study	N/A
Critical commercial assays		
4–20% Mini-PROTEAN® TGX Stain-Free™ Protein Gels, 15 well, 15 µl	Bio-Rad	Cat# 4568096
Clarity Max Western ECL Substrate, 100 ml	Bio-Rad	CAT# 1705062
Restore™ Western Blot Stripping Buffer	Thermo Fisher	CAT# 21059
Experimental models: Organisms/strains		
Mouse: C57BL/6J male	Jackson Laboratories	Strain # 000664; RRID:IMSR_JAX:000664
Software and algorithms		
Vevo Lab v5.2.6	FujiFilm Visualsonics	https://www.visualsonics.com/product/software/vevo-lab
PVAN	Millar Instruments	https://www.adinstruments.com/support/downloads/windows/pvan
ParaVision v6.01	Bruker Inc.	https://www.bruker.com/en/products-and-solutions/preclinical-imaging/paravision-360.html
3D Slicer	N/A	www.slicer.org
GraphPad Prism v8.0	GraphPad Software	https://www.graphpad.com/scientific-software/prism/
Image Lab v6.1.0	Bio-Rad	https://www.bio-rad.com/en-us/product/image-lab-software?ID=KRE6P5E8Z
Other		
Galactic Cosmic Rays (GCR)	Brookhaven National Laboratory	N/A
J. L. Shepherd Mark I Model 68A ^{137}Cs Gamma Irradiator	J. L. Shepherd & Associates	N/A
Histology Services	Duke Pathology Research Immunohistology Lab	N/A

RESOURCE AVAILABILITY

Lead contact

Further information and requests for resources (such as mouse tissue requests) should be directed to the lead contact, Dawn E. Bowles, Ph.D. (dawn.bowles@duke.edu).

Materials availability

This study's biobanked mouse organs are stored within the Bowles Lab at Duke University

Data and code availability

- This study did not generate new standard datastes. Raw Data supporting the conclusions of the paper will be made publically available through NASA's Life Sciences Data Archive (LSDA) data archives. The data can be accessed after 2 years through the following link (http://lsda.jsc.nasa.gov). In the meantime, requests to access data presented in this paper can be directed to the lead contact
- This paper did not utilize nor generate original code
- Any additional information required to reanalyze the data reported in this work paper is available from the lead contact upon request

EXPERIMENTAL MODEL AND SUBJECT DETAILS

Experimental animals

All animal experiments were approved by the Duke University and Brookhaven National Laboratories's Institutional Animal Care and Use Committees (IACUCs). Approximately 24 week old C57BL/6 male mice (Jackson Laboratories) underwent baseline echocardiograms at Duke University before transfer to NSRL at BNL for radiation experiments. Mice were housed together with their littermates at all times throughout the study. They were allowed an acclimation period of 2–4 days a few days prior to radiation exposure. Some mice were exposed to gamma radiation using the J. L. Shepherd Mark I Model 68A ^{137}Cs Gamma irradiator at BNL. Other animals were exposed to ^{16}O (600 MeV/n), ^{56}Fe (1,000 MeV/n), or $GCR_{5\text{-ion}}$ using the beam line at NSRL. Finally, control animals were placed in equitable radiation holders over a schedule, which mimicked the experimental groups. Since $GCR_{5\text{-ion}}$ exposure took a longer period of time than single mono-energetic ions, a set of age matched $GCR_{5\text{-ion}}$ controls were created that are analyzed separately from the single mono-energetic ion or gamma controls. Post-radiation, animals were allowed at least 2 days to recover, and then were returned to Duke University animal facilities where they underwent their longitudinal cardiac assessments.

METHOD DETAILS

Transthoracic echocardiograms

All echocardiograms were performed at the Duke Cardiovascular Physiology Core using a VisualSonics Vevo3100 echocardiography machine with 30 mHz probe and analyzed using Vevo Lab software (version 5.2.6). Prior to obtaining baseline TTE, mice were pre-conditioned the day before by being held in the same manner during shaving as they would be held during the echocardiogram, to decrease stress during the procedure. Next, mice underwent conscious echocardiography by an experienced technologist. All echocardiogram images were assigned a code based on experimental group and uploaded to a centralized server. To ensure rigor and reproducibility, each echocardiogram was interpreted by two independent blinded experienced readers, and their readings were averaged to give a final value. To ensure accuracy, interobserver differences in fractional shortening were assessed amongst all treatment arms and these differences were found to be normally distributed. A "significant" discrepancy was defined as interobserver difference that was greater than two standard deviations from the mean interobserver difference, which was found in 10% of all echocardiograms. Studies with a significant discrepancy between two readers underwent a third analysis by another reader, and the final value is a reflection of three reads. The parameters that were measured on echocardiograms are listed in Table S2.

Pressure-volume loop (PVL) assessments

A subset of animals underwent PVL assessment. All PVL procedures and analyses were performed at the Duke Cardiovascular Research Center by an experienced microsurgeon based on methods reported in the literature (Yoo et al., 2009; Abraham et al., 2016, 2018). Parallel conductance (Vp) of the blood pool was determined by 10-μL injection of 15% saline into the right jugular vein. The derived Vp was used to correct the pressure-volume loop data. Data were recorded digitally at 1,000 Hz and analyzed with pressure-volume analysis software (PVAN data analysis software version 3.3; Millar Instruments). Mice that died after receiving anesthesia or became hypotensive during the course of the protocol, suggesting a surgical complication (LV rupture, bleeding, arrhythmias), were excluded. A small laparotomy was performed, and the inferior vena cava occluded to decrease preload to the heart in order to measure load independent parameters. After completion of the PVL measurements, the animals were euthanized, tissue isolated, and bio preserved as described previously (Brown et al., 2020). Analysis and interpretation of the PVLs was done by DA.

Cardiac MRI (cMRI) & image analysis

All cMRI evaluations were performed at the Duke Center for *In Vivo* Microscopy. Imaging was performed on a 7.0 T Bruker Biospec small animal MRI scanner (Bruker Inc., Billerica, MA). Animal anesthesia was induced and maintained with inhaled isoflurane (0.5–2.0%), and breath rate was monitored for the duration of the scans. Animals were positioned on a custom 3D-printed bed and body temperature was maintained with warm water circulation. The animals were maintained on isoflurane for less than an hour, to reduce drops in cardiac function as a result of prolonged sedation. The animals were recovered after the completion of cMRI image acquisition.

Images were acquired with ParaVision® 6.0.1 platform (Bruker Inc.) using a 4-channel surface coil array (inverted mouse brain coil) combined with a 72mm diameter actively decoupled linear volume coil for transmission. Cardiac time-course images were acquired using an intra-gated multi-slice T1-weighted cine FLASH sequence (TE/TR = 2.0/88.6 ms; 0.1 × 0.1 × 0.8 mm voxel size; 8 slices; 12 frames/cardiac cycle), with the addition of a bright-blood pulse to enhance blood pool signal without the need for an injected contrast agent. Slice orientation was adjusted to take serial slices perpendicular to the long axis of the heart, such that the 0.1 mm^2 in plane slices demonstrated cross-sections of the LV, which was verified by a cardiac clinician (MB).

Images were analyzed using 3D Slicer open source image analysis software (www.slicer.org), as well as Image J (https://imagej.nih.gov). At each time point throughout the cardiac cycle, LV volume was measured by manual segmentation of each slice. Cardiac wall thickness was measured using Image J, with the location standardized using the papillary muscles. Linear distances were measured in six radial positions across the LV at peak systole and diastole, and all measurements were performed in triplicate to assess measurement precision.

Tissue histology

Mice were euthanized through a bilateral thoracotomy and secondary exsanguination. A gravity perfusion rig was set up by elevating a flask containing 4% PFA to a height of ~150cm above the mouse body. The flask was connected to tubing fitted with a 22G hypodermic needle at the end. While the heart was still beating, the needle was inserted *in situ* into the left ventricle to a depth of ~5mm and 4% PFA was allowed to flow. Perfusion was continued until blanching of the heart and liver and contraction of skeletal muscle was observed. Hearts and aortas were then excised and left for further fixation overnight in 4% PFA at 4°C. The following day, all samples were transferred into PBS pH 7.4 and sent to Duke Pathology Research Immunohistology Lab for paraffin embedding, transverse (short axis) 5μm serial sectioning, and Hematoxylin & Eosin (H&E) and Masson Trichrome staining (MT).

A board-certified, cardiac fellowship trained surgical pathologist (CG) evaluated all H&E and corresponding MT stained slides in a de-identified fashion. All histologic sections were reviewed for the absence or presence of aortic medial necrosis (defined histologically by disruption of collagen, dropout of smooth muscle cell nuclei and increased basophilic ground substance), medial degeneration, and elastin fragmentation (defined histologically by a disruption in the organized, linear architecture of the parallel elastic fibers within the wall of the aortic medial layer) and architectural distortion. All histologic sections were reviewed for the absence or presence of common disorders in cardiac and aortic pathology, which includes endocardial, interstitial, or replacement fibrosis, active myocarditis, granulomatous inflammation, amyloidosis, myocyte disarray, myocardial infarction, aortic dissection, or accelerated atherosclerosis.

Western Blot & densitometric analysis

Heart apex samples were homogenized using a glass dounce in 300 μL of TBST + proteinase inhibitor solution. All samples were centrifuged at 13,000 rpm in a microcentrifuge for 10 min. Supernatants were carefully transferred to clean microcentrifuge tubes and protein content quantified using a BCA assay (Thermo Fisher Scientific). For each sample, 60 μg of protein were loaded per well into stain-free 4–20% Tris-Glycine polyacrylamide gels (Bio-Rad). Two lanes of Thermo Fisher Spectra™ Multicolor Broad Range Protein Ladder were also loaded such that they flanked the samples. Gels were run at 100V for 75 min or until the the dye-front reached the marker on the gel cassette.

0.2 μm PVDF membranes were soaked in ice-cold 100% MeOH for 3 min and then transferred to a 10% MeOH Transfer Buffer. Filter paper and sponges were also presoaked in Transfer Buffer while the gel

was running. Gel with protein was equilibrated in ice-cold 10% MeOH Transfer Buffer for 10 min before assembling in a wet-transfer tank with the PVDF membrane, filter paper, and sponges. Proteins were transferred to the membrane at 30V for 30 min in 10% MeOH Transfer Buffer. Post-transfer, the membrane was incubated in 2.5% non-fat milk (w/v) in TBST overnight at 4°C. The gel was imaged using Bio-Rad's stain-free technology and Chemidoc™ MP imager to determine if protein transfer was sufficient, indicated by an absence of visible bands on the gel.

Indirect detection was implemented for probing the blot for protein using the following primary antibodies: anti- Fibulin 4 (Thermo Fisher | BS-13059R), Fibulin-5 (Thermo Fisher | 12188-1-AP), TGF-β1 (Abcam | ab215715), eGFR (Abcam | ab52894), and TBP (Abcam | Ab220788). All primary antibodies used the same secondary antibody, goat HRP conjugated anti-Rabbit IgG (Bio-Rad | 1706515). Primary antibodies and secondary antibody were incubated at RT for 2 h and 1 h, respectively, in 2.5% non-fat milk TBST with 45 rpm shaking. In between antibody incubations, blots were washed three times 10 min each with 10 mL of TBST with 45 rpm shaking at RT.

Blots were visualized using Clarity Max ECL detection reagent (Bio-Rad). Blots were washed with 10 mL of TBST as mentioned above and incubated with detection reagent for 5 min at RT with 45 rpm shaking. Blots were visualized for colorimetric detection of protein ladders and chemiluminescent detection of probed targets. Blots were stripped of antibodies by incubating at 37°C with 30 mL of Restore™ Western Blot Stripping Buffer (Thermo Fisher) with occasional agitation. Stripped blots were then re-probed, after extensive TBST washing and subsequent blocking, using the methods described above.

TIFF image files of probed blots were loaded into Image Labs v6.1.0 (Bio-Rad) for densitometric analysis. Every sample's intensities were normalized to TBP to retrieve adjusted intensities. Molecular weight analysis was also implemented to identify target bands for statistical analysis.

QUANTIFICATION AND STATISTICAL ANALYSIS

For analyses comparing multiple groups (single mono-energetic ion studies), Nonparametric one-way ANOVA (Kruskal-Wallis Test) followed by Dunnett's multiple comparisons test was performed. For studies comparing $GCR_{5\text{-ion}}$ to unirradiated controls, nonparametric Mann-Whitney test, two sided was used. For survival curve analyses among multiple groups, Log-rank (Mantel-Cox) test was performed. Western blot densitometric analysis comparing $GCR_{5\text{-ion}}$ to unirradiated controls used two-sided unpaired t-tests. GraphPad Prism version 8.0 was used for making data visualization and for statistical analysis. Significance was considered at $p \leq 0.05$.